Axisymmetric Bubble Pinch-Off at High Reynolds Numbers

J. M. Gordillo*

Área de Mecánica de Fluidos, Departamento de Ingeniería Energética y Mecánica de Fluidos, Universidad de Sevilla, Avenida de los Descubrimientos s/n, 41092 Sevilla, Spain

A. Sevilla,† J. Rodríguez-Rodríguez,‡ and C. Martínez-Bazán§

Departamento de Ingeniería Térmica y de Fluidos, Universidad Carlos III de Madrid, Avenida de la Universidad 30, 28911 Leganés, Madrid, Spain

(Received 29 June 2005; revised manuscript received 14 September 2005; published 1 November 2005)

Analytical considerations and potential-flow numerical simulations of the pinch-off of bubbles at high Reynolds numbers reveal that the bubble minimum radius, r_n, decreases as $\tau \propto r_n^2\sqrt{-\ln r_n^2}$, where τ is the time to break up, when the local shape of the bubble near the singularity is symmetric. However, if the gas convective terms in the momentum equation become of the order of those of the liquid, the bubble shape is no longer symmetric and the evolution of the neck changes to a $r_n \propto \tau^{1/3}$ power law. These findings are verified experimentally.

DOI: 10.1103/PhysRevLett.95.194501 PACS numbers: 47.55.Dz, 47.20.Ft, 47.20.Ky

The mechanisms underlying the capillary driven breakup of drops or liquid threads in a gas environment have been precisely described and experimentally verified during the last decade [1–4]. However, despite its obvious relevance in many industrial applications, the generation and breakup of bubbles has received less attention in the literature. Therefore, the purpose of this Letter is to contribute to the understanding of the final stages of bubble pinch-off at high Reynolds numbers.

It is well known that, under inviscid conditions, the pinch-off dynamics of droplets is governed by a *local* balance between surface tension forces and inertia (hereafter, inertia will refer to the material derivative of linear momentum, $\rho Du/Dt$). Therefore, the near field structure of drop pinch-off is self-similar and *universal*, in the sense that it does not depend on either initial or far field flow conditions. Moreover, Refs. [2,5] reported that the interface had a self-similar, highly asymmetric double-cone shape at times close to the finite-time singularity.

On the other hand, recent experiments of bubble breakup in a highly viscous liquid [6] have confirmed previous experimental and numerical results [7,8], which clearly showed that the low Reynolds number breakup of bubbles is symmetric, and that the minimum radius approaches to zero linearly with τ. In addition, Suryo *et al.* [8] reported that the local shape of the interface near the singularity is parabolic and that the pinch-off is not self-similar. However, the case of bubble breakup in a low viscosity liquid (e.g., air in water), under study in the present work, seems to be slightly more subtle than its viscous counterpart. Indeed, Leppinen and Lister [5] found that, under the assumption of potential flow, the self-similar solution near pinch-off is no longer stable when $\Lambda < 1/6.2$, where $\Lambda = \hat{\rho}_g/\hat{\rho}_l$ is the inner (gas in our case) to outer (liquid in our case) density ratio. Moreover, in the study by Leppinen and Lister, the radius of the neck, r_n, behaves as $\tau^{2/3}$ for $\tau \to 0$. Nevertheless, recent accurate experimental measurements reported in [6] show that r_n behaves as $\tau^{1/2}$ for $\tau \to 0$, in agreement with previous analytical predictions [9]. The reason for the different exponent in the power law given in [5] and that of [6,9] lies in the fact that, whereas in the former study the pinch-off is promoted by surface tension, in the latter it is solely driven by the liquid inertia. Consequently, in this Letter we try to solve the apparent contradictions found by the above mentioned studies presenting both experimental evidences and potential-flow numerical simulations similar to those reported in [10,11], respectively, and we propose a slight correction to the above mentioned $r_n \propto \tau^{1/2}$ law.

Previous numerical results [11] show that a bubble breaks up symmetrically when it is placed at the stagnation point of a straining flow given by the following dimensionless velocity potential ϕ at infinity

$$\phi = -1/8r^2 + 1/4z^2, \tag{1}$$

where r and z are the dimensionless radial and axial cylindrical coordinates, respectively. Here, distances, velocities, and densities have been made dimensionless using $\hat{R}$ (initial bubble radius), $\hat{U}_l$ (characteristic outer flow velocity), and $\hat{\rho}_l$, respectively, and dimensional variables are indicated by a hat accent. The numerical method used to solve the coupled system of the Laplace and Bernoulli equations that govern the gas flow inside the bubble and the outer liquid flow can be briefly described as follows. Provided the values of the inner and the outer potentials along the free surface at a given time, the velocities normal to the interface are computed through a boundary integral method that solves the discretized version of both the liquid and the gas Green integral equations. The values of the potentials are explicitly updated in time making use of a modified version of Bernoulli's equation that takes into account both the inner and the outer fluid densities, whereas the new positions of the nodal points are obtained

by moving them normal to the interface. A more detailed description of the numerical method can be found in [11]. With the aim of establishing the appropriate dependence of r_n on τ, we carried out numerical simulations of the evolution of the interface of a bubble initially located within the straining flow given by Eq. (1) either at $r = 0$, $z = z_0 = 0$ (*symmetric* case) or at $r = 0$, $z = z_0 > 0$ (*asymmetric* cases). In our simulations we considered two different values of the inner to outer density ratio, namely, $\Lambda = 1.2 \times 10^{-3}$ and $\Lambda = 1.2 \times 10^{-4}$.

Figure 1 shows that, in the symmetric case, the local bubble shape near the singularity is a parabola. It can be inferred from Fig. 1(a) that the radial length scale decreases more rapidly than the axial one, and consequently, the region near the singularity can be considered slender. Thus, to determine the proper dependence of r_n on τ, the analysis of the free-surface, potential-flow problem simplifies to solve the following ordinary differential equation when $r_n \ll 1$:

$$\ln r_n (r_n' r_n)' + \frac{1}{2}(r_n')^2 = 0. \tag{2}$$

Integration of Eq. (2) gives $A\tau = r_n^2\sqrt{-\ln r_n^2} \times [1 + O((\ln r_n^2)^{-1})]$, indicating that the dimensionless flow rate per unit length, $q = r_n' r_n$, is such that $q \to 0$ as $\tau \to 0$. Notice that our analytical result provides a dependence of r_n on τ with a slope, in a log-log scale, larger than $1/2$, but which monotonically decreases towards $1/2$ for $\ln r_n \to -\infty$. Figure 2 shows how the numerical evolution matches the asymptotic behavior $\tau \propto r_n^2\sqrt{-\ln r_n^2}$ for $\tau < 0.01$, which slightly differs from the $r_n \propto \tau^{1/2}$ power law reported in [6,9]. It needs to be pointed out that the deviation from the $1/2$ power law has been previously experimentally measured at the Physics of Fluids group at Twente University. Finally, it should be pointed out that, since $\hat{\rho}_l \hat{q}/\hat{\mu}_l \to 0$ for $\tau \to 0$, the liquid viscosity must be retained to describe the latest instants prior to pinch-off.

The local behavior in the asymmetric cases, displayed in Fig. 1(b), differs from its symmetric counterparts in that the interface tends to form a double cone with different semiangles. Furthermore, Fig. 2 shows that this type of breakup leads to $r_n \propto \tau^{1/3}$ at the latest instants of pinch-off.

The existence of the $1/3$ power law can be physically explained as follows. Whereas the symmetry imposes a zero gas velocity inside the neck ($v_g = 0$), in the asymmetric breakup v_g increases as $\tau \to 0$, as shown in Fig. 3. Thus, as the gas flows through the neck at a velocity v_g, there is a suction originated by the high-speed gas stream (Bernoulli's effect), which further accelerates the outer liquid towards the axis, explaining the faster asymmetric collapse.

In the following, we will show that the $1/3$ power law appears because the final stages of pinch-off are not driven by either surface tension or liquid inertia solely, but by both liquid and gas inertia. First, note that dimensional argu-

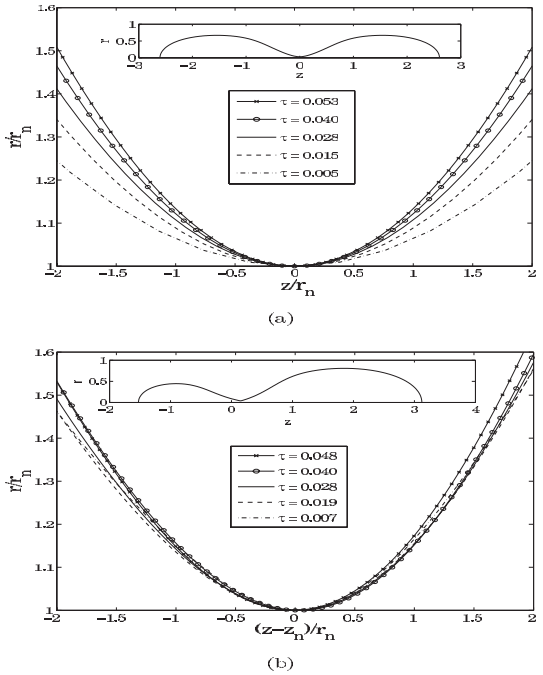

FIG. 1. Time evolution of the pinch-off region of a bubble, $\Lambda = 1.2 \times 10^{-3}$, at $We = \hat{\rho}_l \hat{U}_l^2 \hat{R}/\hat{\sigma} = 12$. In both cases, the number of discrete points along the interface (513) were rearranged at every time step in order for them to be equispaced. (a) Symmetric breakup ($z_0 = 0$) and (b) asymmetric case ($z_0 = 0.25$). Note that, while in (a) the radial scale is stretched more rapidly than the axial one, (b) suggests that a self-similar solution could be reached near the pinch-off time if the Kelvin-Helmholtz (shear) instabilities were prevented.

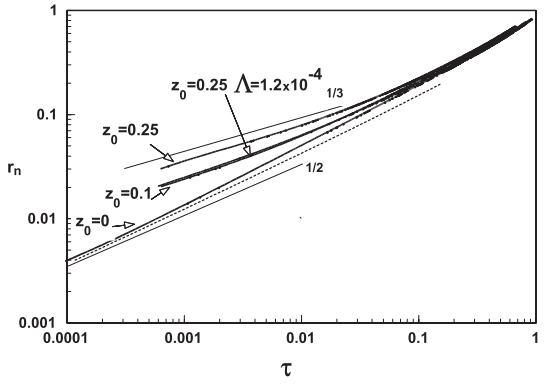

FIG. 2. Time evolution of the radius of the neck, $r_n(\tau)$, for different values of z_0 and Λ (otherwise stated, $\Lambda = 1.2 \times 10^{-3}$ at $We = \hat{\rho}_l \hat{U}_l^2 \hat{R}/\hat{\sigma} = 12$). Notice that the transition from the approximately $1/2$ to the $1/3$ power law is delayed as Λ and/or Q_g decrease. The results given for $z_0 = 0.25$, $\Lambda = 1.2 \times 10^{-4}$ ($Q_g \simeq 0.59$, $q \simeq 0.197$, $r_{\text{tran}} \simeq 3.3 \times 10^{-2}$) and those given for $z_0 = 0.1$, $\Lambda = 1.2 \times 10^{-3}$ ($Q_g \simeq 0.26$, $q \simeq 0.21$, $r_{\text{tran}} \simeq 4.3 \times 10^{-2}$) are almost identical since the values of r_{tran} are nearly the same in both cases. The dashed line represents $\tau = 2.2 \times r_n^2\sqrt{-\ln r_n^2}$.

ments require a typical length to determine the characteristic gas velocity in our potential-flow problem, which cannot be the capillary one since surface tension effects are negligible in a collapse following a 1/3 power law [$We_n = \hat{\rho}_l(d\hat{r}_n/d\hat{\tau})^2\hat{r}_n/\hat{\sigma} \propto \tau^{-1}$, $\hat{\sigma}$ being the liquid-gas surface tension]. The solution to this apparent paradox is given by a quick inspection of Fig. 3, where it is shown that, in our incompressible, inviscid simulations, and within admissible numerical errors, $v_g r_n^2 = Q_g \simeq$ const, where Q_g stands for the dimensionless gas flow rate. Thus, the balance between the liquid inertia, $\hat{\rho}_l D\hat{u}_l/Dt$, and the pressure drop in the gas stream requires that $\hat{\rho}_l\hat{r}_n/\hat{\tau}^2 \sim \hat{\rho}_g\hat{Q}_g^2/\hat{r}_n^5$, indicating that r_n and v_g can be appropriately defined as $r_n \sim \Lambda^{1/6}Q_g^{1/3}\tau^{1/3}$ and $v_g \sim \Lambda^{-1/3}Q_g^{1/3}\tau^{-2/3}$, respectively. Note that, in the above discussion of the asymmetric case ($Q_g \neq 0$), we have considered the gas flow to be quasisteady since the gas residence time, $\hat{t}_r \sim \hat{r}_n^3/\hat{Q}_g$, is much smaller than the characteristic time of the problem, $\hat{t}_0$, which can be either $\hat{t}_0 \sim \hat{r}_n^2/\hat{q}$ or $\hat{t}_0 \sim \hat{r}_n^3/\hat{Q}_g\Lambda^{-1/2}$ and thus $t_r/t_0 \sim r_n(q/Q_g) \ll 1$ or $t_r/t_0 \sim \Lambda^{1/2} \ll 1$. Also notice that the transition to the 1/3 power law will take place at a characteristic transition radius r_{tran} such that the liquid and the gas inertia are both of the same order of magnitude, $\hat{\rho}_l(\hat{q}/\hat{r}_{\text{tran}})^2 \sim \hat{\rho}_g(\hat{Q}_g/\hat{r}_{\text{tran}}^2)^2 \rightarrow r_{\text{tran}} \sim \Lambda^{1/2}[Q_g/q(\tau)]$. Clearly, the smaller $Q_g/q(\tau)$ is for $\tau \sim O(1)$ (or, equivalently, the smaller the initial asymmetry), the smaller the transition radius is and the more difficult it will be to determine, either numerically or experimentally, the existence of the 1/3 power law. This conclusion is supported by Fig. 2, where it is shown that, under the potential-flow approximation, this transition exists whenever there is an initial asymmetry ($z_0 = 0.10$ and $z_0 = 0.25$). Consistent with the above discussion, in the symmetric case no transition is observed within the spatial resolution of our numerical method. Furthermore, the power law transition is delayed as Λ or Q_g decrease (see Figs. 2 and 3). Figure 2 also shows that, in the case of $z_0 = 0.25$, the transition radius is smaller for $\Lambda = 1.2 \times 10^{-4}$ than that obtained for $\Lambda = 1.2 \times 10^{-3}$. It should also be emphasized that neither Q_g nor q are fixed locally, but through the entire flow domain.

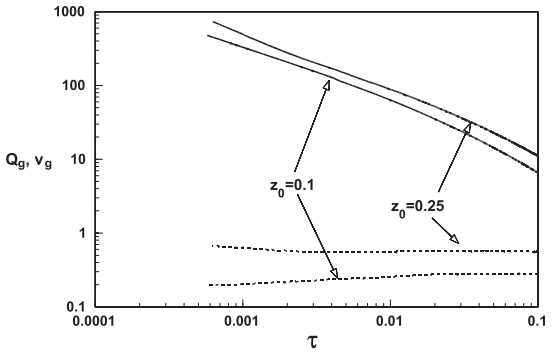

FIG. 3. Time evolution of Q_g (dashed lines) and v_g (solid lines) for $z_0 = 0.25, 0.1$, $\Lambda = 1.2 \times 10^{-3}$, and $We = 12$. It can be observed that, whereas v_g increases almost two decades, Q_g remains nearly constant during the breakup process.

So far we have assumed that the characteristic axial length scale near the singularity is the same as the characteristic radial length scale, i.e., r_n. However, as pointed out in [5], the strong shear near the minimum radius favors the development of a Kelvin-Helmholtz instability, for which all the lengths greater than δ_m, with $\delta_m \sim (Q_g^2 We\Lambda)^{-1} r_n^4 \ll r_n$ being the characteristic dimensionless length scale such that surface tension and gas inertia are both of the same order of magnitude, will be unstable. Here, $We = \hat{\rho}_l\hat{U}_l^2\hat{R}/\hat{\sigma}$ and, consequently, if the latest instants previous to break up could be accurately simulated, dendrites of a typical length scale $\delta_m \ll r_n$, analogous to the ones identified in [5], would develop.

The applicability of the above results to real flows depends on the validity of the potential-flow approximation employed here. Although the thickness of the gas viscous boundary layer $\delta_g \sim r_n Re_g^{-1/2} \propto r_n^{3/2}$, where $Re_g = \hat{\rho}_g\hat{Q}_g/(\hat{\mu}_g\hat{r}_n)$, is very small compared with the radius of the neck, $\delta_g \ll r_n$, flow separation may take place downstream from the axial location of r_n. Indeed, in a first approach, the gas flow downstream of the neck is quasisteady and similar to that of a divergent diffuser with some blowing at the walls, whose opening semiangle is larger than the separation one. Under these conditions the flow may separate, avoiding the gas stagnation pressure to fully recover inside the growing bubble. Furthermore, the flow separation will decrease the above mentioned suction effect and, consequently, $\hat{Q}_g$ will also decrease, producing a subsequent accumulation of gas upstream of the neck. To conclude, the suction mechanism, which accelerates the outer liquid radially toward the axis, will be less effective in real flows than it is predicted by our simulations. In addition, viscous effects in the liquid are expected to be negligible since $Re_l \propto \tau^{-1/3}$.

Up to now we have presented our numerical results to describe the time evolution of the neck during the bubble breakup process. However, in addition to the numerical simulations we have also performed a meticulous series of experiments of bubble formation in a coflowing liquid stream using the experimental facility described in [10]. To study the final stages of the bubble breakup, we used a high-speed video camera to record sequences of the breakup of bubbles at a rate which was varied between 3×10^4 frames/s (resolution of 256×128 pixels) and 5×10^4 frames/s (resolution of 256×64 pixels) depending on the experimental conditions. An example of two different sequences are shown in Fig. 4. Before we proceed any further, we would like to mention that the experiments reported here were previously selected to make sure that the breakup was purely axisymmetric. Figure 5 shows the neck radius evolution as it approaches the singularity (pinch-off point). This figure reports an experimental evidence of the $r_n \sim \tau^{1/3}$ power law in spite of flow separation. As already discussed, the clear departure from the 1/2

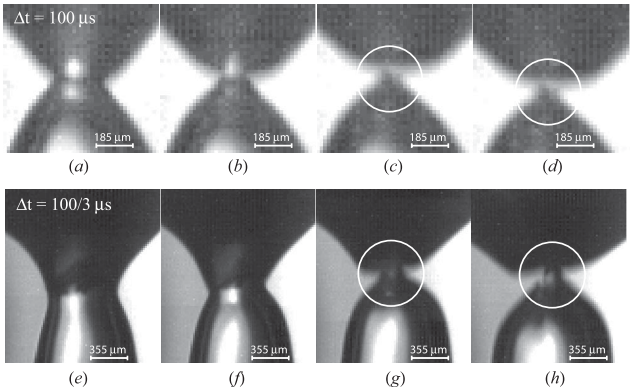

FIG. 4. Close-up views showing two different sequences of the bubble pinch-off corresponding to the experimental conditions of Fig. 5. The air and water flow rates are $Q_a = 610$ ml/min, $Q_w = 4$ l/min in photographs (a)–(d), and $Q_a = 850$ ml/min, $Q_w = 6$ l/min in (e)–(h). The time interval between the shown frames is $\Delta t = 100$ μs in (a)–(d), and $\Delta t = 100/3$ μs in (e)–(h). The spatial resolution is, in all cases, 18.6 μm/pixel, and the movies were recorded with a shutter time of $1/30\,000$ s^{-1}. Gas and liquid Reynolds numbers based on the needle diameter are, for both experimental conditions, of the order of $\sim O(10^3)$ and $\sim O(10^4)$, respectively.

power law is promoted by the favorable (negative) pressure gradient induced by the gas flow towards the neck. The breakup time was determined from the recordings by least-squares fitting of the last 6 to 10 data points to the 1/3 power law, since fitting to the $\tau \propto r_n^2\sqrt{-\ln r_n^2}$ or to the 2/3 power law resulted in inconsistent results for the pinch-off time when compared to the high-speed movies. It was checked that the results were not sensitive to the number of selected data points and, in all cases, the correlation

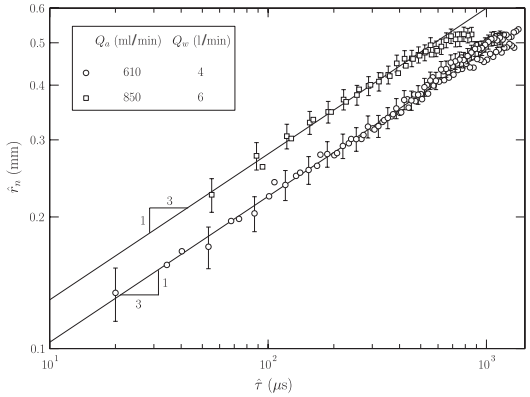

FIG. 5. Experimental results for the evolution of $\hat{r}_n$ with $\hat{\tau}$ in a coflowing air-water jet. The gas is injected through a needle (inner and outer radii 0.419 and 0.635 mm, respectively) placed coaxially within a liquid jet discharging from a 4 mm radius circular nozzle. Q_a and Q_w denote the air and water flow rates, respectively. A detailed description of the experimental facility is given in [10].

coefficient was very close to unity. More importantly, the photographs shown in Fig. 4 provide evidence of the strong asymmetry generated by the favorable pressure gradient induced by the gas flow in the neck region [see frames (c), (d), (g), and (h) in Fig. 4].

In view of the previous results, it can be concluded that, in spite of flow separation, the favorable pressure gradient generated accelerates the liquid both radially and axially, producing a strong asymmetry near the neck region. Since this mechanism is only appreciable at scales $r_{\text{tran}} \sim \Lambda^{1/2}(Q_g/q)$, detailed experiments need to be carried out in order to verify whether this behavior, experimentally verified for large values of Q_g/q, is also present if, for $\tau \sim O(1)$, $Q_g/q(\tau) \lesssim O(1)$.

The authors are grateful to the PoF group at Twente University, Enschede, The Netherlands, and especially to Professor Detlef Lohse, for their hospitality and for sharing with us their experimental results. We also wish to thank the Department of Continuum Mechanics and Structural Analysis, UC3M, for sharing their high-speed camera with us. This research has been supported by the Spanish MCyT under Projects No. DPI2002-04550-C07-06 and AGL2000-0374-P4-02.

*Electronic address: jgordill@us.es
†Electronic address: asevilla@ing.uc3m.es
Present address: Department of Applied Physics, University of Twente, P.O. Box 217, 7500 AE Enschede, The Netherlands.
‡Electronic address: fjrodriguez@ucsd.edu
Present address: Department of Mechanical and Aerospace Engineering, University of California, San Diego, 9500 Gilman Drive, La Jolla, CA 92093-0411, USA.
§Electronic address: cmbazan@ujaen.es
Present address: Área de Mecánica de Fluidos, Universidad de Jaén, Campus de las Lagunillas, 23071 Jaén, Spain.

[1] J. Eggers, Rev. Mod. Phys. **69**, 865 (1997).
[2] R. F. Day, E. J. Hinch, and J. R. Lister, Phys. Rev. Lett. **80**, 704 (1998).
[3] A. Chen, P. Notz, and O. A. Basaran, Phys. Rev. Lett. **88**, 174501 (2002).
[4] J. Eggers, Z. Angew. Math. Mech. **85**, 400 (2005).
[5] D. Leppinen and J. R. Lister, Phys. Fluids **15**, 568 (2003).
[6] J. Burton, R. Waldrep, and P. Taborek, Phys. Rev. Lett. **94**, 184502 (2005).
[7] P. Doshi *et al.*, Science **302**, 1185 (2003).
[8] R. Suryo, P. Doshi, and O. Basaran, Phys. Fluids **16**, 4177 (2004).
[9] M. S. Longuet-Higgins, B. R. Kerman, and K. Lunde, J. Fluid Mech. **230**, 365 (1991).
[10] A. Sevilla, J. M. Gordillo, and C. Martínez-Bazán, J. Fluid Mech. **530**, 181 (2005).
[11] J. Rodríguez-Rodríguez, J. M. Gordillo, and C. Martínez-Bazán, J. Fluid Mech. (to be published).